Biochemistry and Biophysics Reports 42 (2025) 101975

Contents lists available at ScienceDirect

Biochemistry and Biophysics Reports

journal homepage: www.elsevier.com/locate/bbrep

In silico studies to understand the interactions of flavonoid inhibitor with nsp12-RNA dependent RNA polymerase of SARS-CoV-2 and its homologs

Shamiya Anwar Kizhakkiniyakath, Tejaswini Choudhury, Madhan Vishal Rajan, Sagar Rathee, Basant Meena [2], Gururao Hariprasad [1,*]

Department of Biophysics, All India Institute of Medical Sciences, Ansari Nagar, New Delhi, 110029, India

ARTICLE INFO

Keywords:
SARS-CoV-2
RNA dependent RNA polymerase
Structure based drug screening
Enzyme inhibition
Flavonoid molecule

ABSTRACT

Aim: COVID 19 continues to be a major health concern. RNA dependent RNA polymerase of *SARS-CoV-2* which is crucial for replication is therefore a potential drug target.
Methodology: Based on experimental structures of RdRp from *SARS-CoV-2*, computational models were generated of its homologs from *SARS-CoV-1*, *MERS* and *Bat. SARS CoV-2* RdRp was used for virtual screening at nucleotide binding site with molecule from COCONUT Natural Products database using Glide. Complexes with the top inhibitor molecule were modelled using Discovery Studio and Desmond suite of programs.
Results: SARS-CoV-2 RdRp has a minimum of 80 % sequence similarity with its homologs, with the secondary structural elements, catalytic residues and metal binding residues being conserved. Certain residue variations in *SARS-CoV-2* RdRp seems to be responsible for the stability of the enzyme. Docking and simulation studies showed that a flavonoid molecule with Coconut ID: CNP0127177.0 (HHF318) has binding affinity in low nanomolar range against RdRp from *SARS-CoV-2* which was comparable or better than currently used inhibitors. This affinity stems from cationic-π with Arg555, and π-stacking interactions with a nucleobase of RNA. Molecule also engages with other residues that are crucial for its functions. This flavonoid molecule has similar physio-chemical properties like ATP towards *SARS-CoV-2* RdRp, and has low potency for human ATP binding proteins.
Conclusion: HHF318 is a potential inhibitor of *SARS-CoV-2* RdRp with good potency, specificity and pharmacokinetic properties for it to be developed as a drug candidate for COVID19.

1. Introduction

COVID19 has been a major global health concern for the last few years. While the pandemic in 2020 caused mortality and morbidity, it continues to be an epidemic that needs to addressed. Though there have been multiple modalities of treatment for COVID19, each approach has been riddled with lacunae [1–14]. From a Biophysical perspective, (1) these nucleoside analogue inhibitors are hindered by the proof reading activity which can excise the incorporated inhibitors conferring resistance to *SARS-CoV-2* [15,16]; (2) Cyano group substituted at the 1' position will sterically clash with side chain of Ser861 preventing translocation of RNA, and a possible mutation at this position may allow processing of RNA synthesis and thereby survival of this virus [17]. Clearly, the clinical compliance of the patients and biophysical pitfalls of nucleoside inhibitors emphasize the need to develop more potent, non-covalently binding non-nucleoside inhibitor molecules.

The replicase gene encoding the non-structural proteins (*nsps*) occupies two-thirds of the genome, about 20 kb, as opposed to the structural and accessory proteins. The replicase polyproteins of the virus comprises of four domains that interact to form RNA Dependent RNA Polymerase (RdRp), that functions in (i) production of negative strand RNA (–RNA); (ii) new genome molecules and, (iii) generation of subgenomic (sg) messenger RNAs (mRNAs) [18–20]. Owing to these important attributes, along with the fact that it lacks a human homologue makes the *SARS-CoV-2* RdRp an important and attractive target for the rational design of potent inhibitory molecules [21–24]. Flavonoid molecules in addition to their diverse structure and drug-relevant features unsurpassable by any synthetic compound, mimic nucleosides making them ideal for a physio-chemical complementarity at the NTP binding site of *nsp12*-RdRp [25–29].

* Corresponding author.
E-mail address: dr.hariprasadg@gmail.com (G. Hariprasad).
[1] GH acknowledges grant A/COVID/2/2020 from All India Institute of Medical Sciences, New Delhi for the grant
[2] BM acknowledges Research section of All India Institute of Medical Sciences, New Delhi for the grant F.No. 1/1-2/JR-SR-Thesis/2023/RS

https://doi.org/10.1016/j.bbrep.2025.101975
Received 9 December 2024; Received in revised form 26 February 2025; Accepted 9 March 2025
2405-5808/© 2025 The Authors. Published by Elsevier B.V. This is an open access article under the CC BY-NC-ND license (http://creativecommons.org/licenses/by-nc-nd/4.0/).

A detailed structural characterization of drug targets is known to be useful in the designing of potent inhibitory molecules [30]. Our group has been actively involved in structure based drug design against targets in microbes causing human infections [31]. In this study, we have conducted comprehensive structural analysis and inhibition studies of the *nsp12*-RdRp of *SARS-CoV-2* using computational methods, exploring natural flavonoids as potential anti-viral agents against *SARS-CoV-2* and its homologs.

2. Methodology

2.1. Sequence analysis

Primary structure of RdRp from *SARS CoV-2* (Accession no.: NC_045512.2) was obtained from NCBI [32]. Homologous sequences were searched using BLAST [33]. Sequences of RdRp from *SARS-CoV-1* (NC_004718.3)*, MERS-CoV* (NC_038294.1) *and Bat-CoV* (NC_048212.1) were selected from NCBI and multiple sequence alignment was done using CLUSTAL-W [34].

2.2. Modelling and validation of the RdRp enzymes and protein preparation

Cryo-EM structure of Replication Transcription Complex of *SARS-CoV-2* bound to ATP, in pre-catalytic state (**PDB Id:** 7UO7) was obtained from 'Research Collaboratory for Structural Bioinformatics-Protein Data Bank' (RCSB PDB) [35]. Structure of RdRp-nsp-12 subunit with primer-template RNA, magnesium and zinc ions was energy minimised. This structure with the mentioned ligands was then validated using PROCHECK, VERIFY 3D and ERRAT and considered for further experiments [36–39]. Homology modelling was performed on RdRp sequences of *SARS-CoV-1, MERS-CoV*, and *Bat-CoV* obtained from the NCBI database to create their respective models based on experimental structures of RdRp from *SARS CoV-2* and *SARS CoV-1* available on RCSB PDB using software tools such as Discovery Studio, Geno 3D, SWISS-MODEL and PHYRE [40–43]. The conformational correctness and reliability of the generated models were analysed using the same validation tools mentioned earlier. Validated structure of RdRp *SARS-CoV-2* with ATP was prepared by adding hydrogen atoms, assigning bond borders and energy minimised using Protein Preparation Wizard from Schrodinger suite [44]. Also, RNA, two zinc ions and one magnesium ion were added to the generated RdRp models of *SARS-CoV-1, MERS-CoV*, and *Bat-CoV* from Discovery Studio and structures were prepared using same methodology.

2.3. Ligand library preparation

ATP and four natural molecules predicted to inhibit RdRp *from SARS-CoV-2* were chosen as scaffold templates [45–47]. A structural similarity search with a Tanimoto coefficient of 0.5 was performed at the COCONUT Natural Products database to shortlist 100 molecules for each of the submitted scaffolds [48]. These molecules were taken up for ligand preparation by generating different stereochemistries, tautomers, and ionization states using LigPrep module of Schrödinger suite [49].

2.4. Virtual screening workflow

Prepared structure of RdRp from *SARS CoV-2* was considered as a receptor with ATP as the centroid for grid generation. This was used to identify possible inhibitors from the curated library using virtual screening workflow program using Glide software from the Schrodinger suite [50,51]. This comprised of an initial library screening using High Throughput Virtual Screening (HTVS). Top 10 % of ranked compounds from this screening were then re-screened using Standard Precision (SP) mode, and the subsequent top 10 % of compounds were further analysed using the Extra Precision (XP) mode. Based on the docking score, top ranked compound amongst these was considered as a potential inhibitor of the enzyme. Dissociation constant (Kd) was estimated using the equation $\Delta G = -nRT.\ln Kd$, where ΔG stands for change in free energy of binding, R stands for gas constant in calorie/mol/Kelvin, T stands for temperature in Kelvin, ln stands for natural log, and n stands for number of moles (calculated for 1 mol).

2.5. Validation of docking methodology

The co-bound ligand (ATP) was extracted from the prepared Cryo-EM structure (PDB Id: 7UO7) while preserving the original co-ordinates. Using the same methodology, ATP was redocked into the binding site of the enzyme. Docked complex was superimposed on the native complex and RMSD was evaluated.

2.6. Preparation of RdRp-Inhibitor model complexes

Co-ordinates of the inhibitor from the complex of RdRp of *SARS-CoV-2* was taken and added to RdRp model structures of *SARS-CoV-1, MERS-CoV*, and *Bat-CoV* using PyMOL [52]. Modelled RdRp-inhibitor complexes from *SARS-CoV-1, MERS-CoV* and *Bat-CoV* RdRp were pre-processed, energy minimised, and taken for further analysis.

2.7. Molecular dynamics

The docked RdRp-Inhibitor complex of SARS-CoV-2 and the RdRp-Inhibitor complexes of homologs obtained through co-ordinate replacement were subjected to molecular dynamics simulation to understand the stability and dynamics of the binding interactions. Simulation was performed using the Desmond suite of programs using the OPLS3 force field parameters [53,54]. RdRp-Inhibitor poses were solvated using the TIP3P explicit water model in an orthorhombic box. Net electrostatic charge on solvated models were neutralized by adding Na^+ and Cl^- ions at a concentrations of 0.15 mol/L. Systems were then subjected to molecular dynamics simulation for 500 ns at a temperature of 300K and a pressure of 1 atm, using the Nose-Hoover thermostat and Martyna-Tobias-Klein barostat [55,56]. The simulation was carried out with a time step of 2 fs (fs), incorporating LINCS harmonic constraints, while the motion was integrated using the RESPA integrator [57,58]. The Simulation Interaction Diagrams program from Schrodinger was utilized for analysis of the trajectories post MD [53].

2.8. Principal Component Analysis (PCA) and free energy landscaping (FEL)

Principal Component Analysis (PCA) of the RdRp-Inhibitor complex trajectories was performed using the MDTraj program [59]. A covariance matrix was constructed from the Cartesian coordinates of the C-α atoms of the protein and the heavy atoms of the ligands. Eigenvalues and eigenvectors of this covariance matrix were computed, enabling the extraction of the ten principal components associated with the eigenvectors that had the highest eigenvalues [60]. A 2D histogram was generated based on Principal Component 1 (PC1) and Principal Component 2 (PC2). The free energy landscape was created from the histogram using the Boltzmann equation: $\Delta E = -k_b\, T \ln(n_i/n_{max})$; where n_i represents the number of conformations in the ith bin, n_{max} indicates the number of conformations in the most populated bin, ΔE denotes the energy difference between these conformations, k_b is the Boltzmann constant, and T is the temperature in Kelvin.

2.9. Docking of top ranked compound to ATP-binding human proteins

Crystal structures of DNA ligase (PDB ID: 6P0D), PI3K (PDB ID: 5DXU), and hexokinase (PDB ID: 1QHA) were retrieved from the RCSB. The ligands were removed from the crystal structures, the proteins were prepared and the inhibitor of RdRp from SARS-CoV-2 was docked at the

Fig. 1. Multiple sequence alignment of RdRp from *SARS-CoV-2* (green), *SARS-CoV-1* (cyan), *MERS-CoV* (pink), *Bat-CoV* (yellow), respectively. Conserved catalytic residues are shown in bold red and cysteine residues are shown in bold yellow. The NCBI accession number and percentage identity is shown at the end of the sequences. The symbol "*" indicates identical residues, ":" indicates conserved substitutions, and "." indicates semi-conserved substitutions.

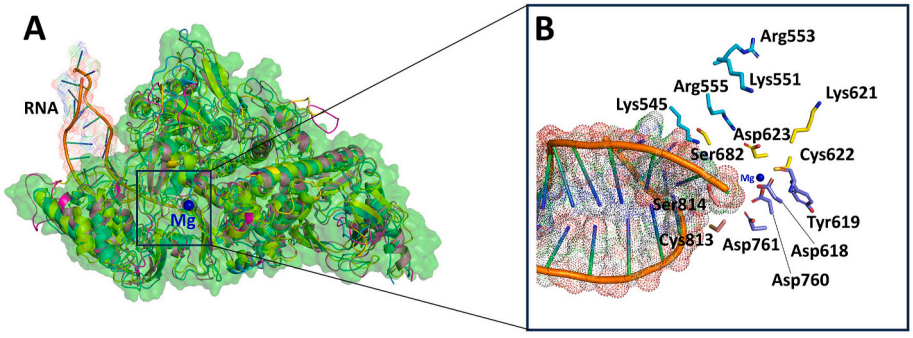

Fig. 2. Overall structural complexes of RdRp enzymes highlighting the structural entities at the active site requisite for functionality. (**A**) GRASP structures of RdRp from *SARS-CoV-2* (green), superimposed with cartoon conformations of RdRp from *SARS-CoV-1* (cyan), *MERS-CoV* (pink), and *Bat-CoV* (yellow). RNA (orange rendering) and Magnesium ion (blue) are shown. (**B**) Residues binding to RNA are shown in cyan; residues involved in NTP recognition are shown in yellow; residues binding to Mg ion are in purple; and residues required for primer RNA binding are in brown.

ATP binding sites using the same methodology mentioned earlier. The docked complexes were then analysed to calculate the Dissociation constant (Kd).

3. Results and discussion

3.1. Sequence analysis of RdRp from SARS-CoV-2 and its homologs

Primary sequences of the RdRp enzymes from *SARS-CoV-2, SARS-CoV-1, MERS-CoV* and *Bat-CoV* show at least 80 % similarity. Understandably *SARS-CoV-1* shares a closer amount of identity as compared to the *MERS-CoV* and *Bat-CoV* sequences (Fig. 1). While key catalytic residues Asp 618 and Asp 623 are conserved on the motif DXXXXD, Ser 759, Asp 760 and Asp 761 are conserved on the motif SDD, on all the four sequences. Though the length of the primary sequences is approximately the same the number of cysteines vary, with *MERS-CoV* having a maximum of 32 and *Bat-CoV* having a minimum of 28. Interestingly only 19 of these are in homologous positions. The enzymes could therefore be

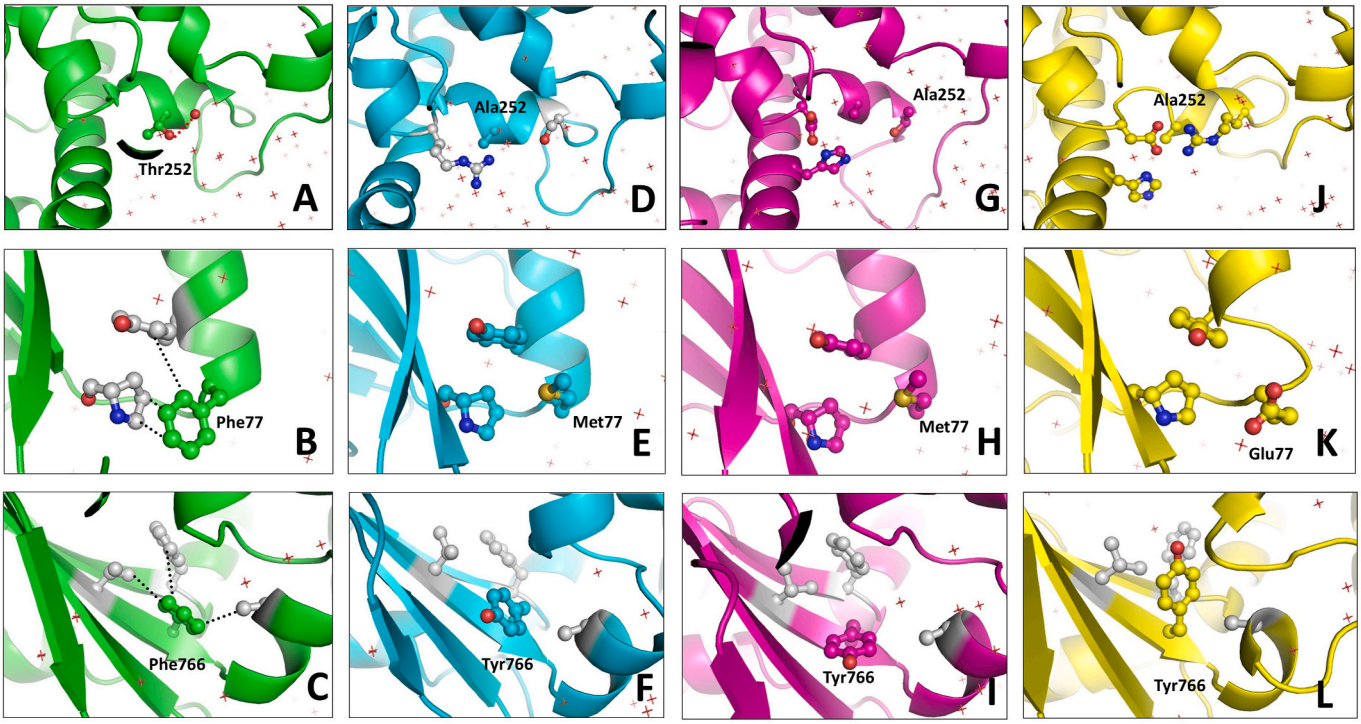

Fig. 3. Comparative analysis at certain analogous residue positions. A-C: *SARS-CoV-2*; **D-F:** *SARS-CoV-1*; **G-I:** *MERS-CoV* virus, and **J-L:** *Bat-CoV*. Hydrogen bonded interactions are shown as red dotted lines and hydrophobic interactions are shown as black dotted lines.

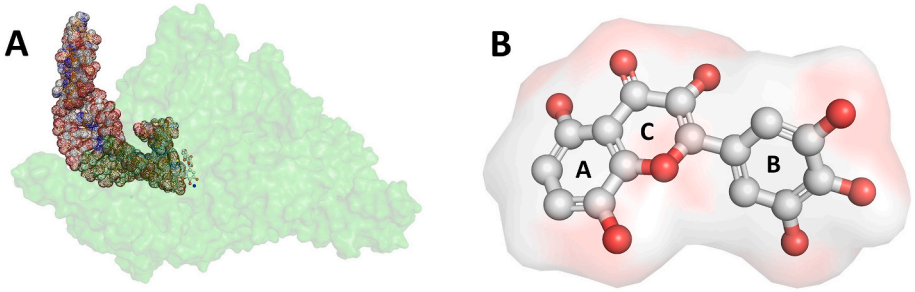

Fig. 4. Structure complex of *SARS-CoV-2* RdRp enzyme with HHF318 (A) HHF318 at the NTP binding site of *SARS-CoV-2* RdRp enzyme with RNA (mesh rendering) and Magnesium (blue sphere), **(B)** Structure of HHF318: 3,3′,4′,5,5′,8-Hexahydroxyflavone.

stabilized by the di-sulphide bond across these cysteines. There are residue variations on the RdRp of *SARS-CoV-2* as compared to the residues conserved on the other three sequences. Notable variations at specific positions, such as Phe77, Val233, Thr252, Lys281, Thr739, Asn743, Phe766, Thr769, and Ser784, may impact the overall stability of the 3D structures, which will be further examined in the structural analysis.

3.2. Modelling of the homologs and validation of RdRp enzymes

Structure of *SARS-CoV-1* RdRp (PDB id: 6NUR), had 161 residues less and so we modelled the complete structure and generated two models. Since *MERS-CoV* and *Bat-CoV* did not have any experimental RdRp structure as of date, they were modelled as well to obtain complete structure and a total of 17 models were generated for each. These structures were evaluated for stereochemical quality and statistical potentials (Table S1). The top models for RdRp from *SARS-CoV-1, MERS-CoV,* and *Bat-CoV* had 99.5 % (926 residues), 99 % (930 residues) and 99.4 % (926 residues) in allowed regions of the Ramachandran plot, respectively. The ERRAT and Verify 3D also shows the accuracy of these models. The energy minimised Cryo-EM structure of *SARS-CoV-2* RdRp (PDB Id: 7UO7) had 99.6 % (926 residues) in the allowed regions of Ramachandran plot, thereby enabling to benchmark the other three generated models.

3.3. Structural analysis of RdRp enzymes

The superimposition of the four RdRp structures showed that RMSD of Cα chains of *SARS-CoV-1* with *SARS-CoV-2* is 1.4 Å, with *MERS-CoV* is 0.9 Å, and with *Bat-CoV* is 1.4 Å (Fig. 2A). This reveals that there are no major variations in the secondary structural features and the minor differences noted are in the flexible loop regions connecting the helices and sheets. Comparative analysis at certain residue positions in RdRp of *SARS-CoV-2* revealed that residues at certain conformations were better suited and made favourable interactions due their inherent biophysical properties and individually contributed to the overall compactness of the protein. Three representative examples of Thr252, Phe77, and Phe766 are provided here for the sake of comparison (Fig. 3).

RdRp from the four viruses *SARS-CoV-2, SARS-CoV-1, MERS-CoV*, and *Bat-CoV* have a multi-domain globular structure comprising of 34–36 alpha helices and 21–23 β-sheets. Conserved catalytic motifs in the RdRp is responsible for the orchestrated movement of the template-

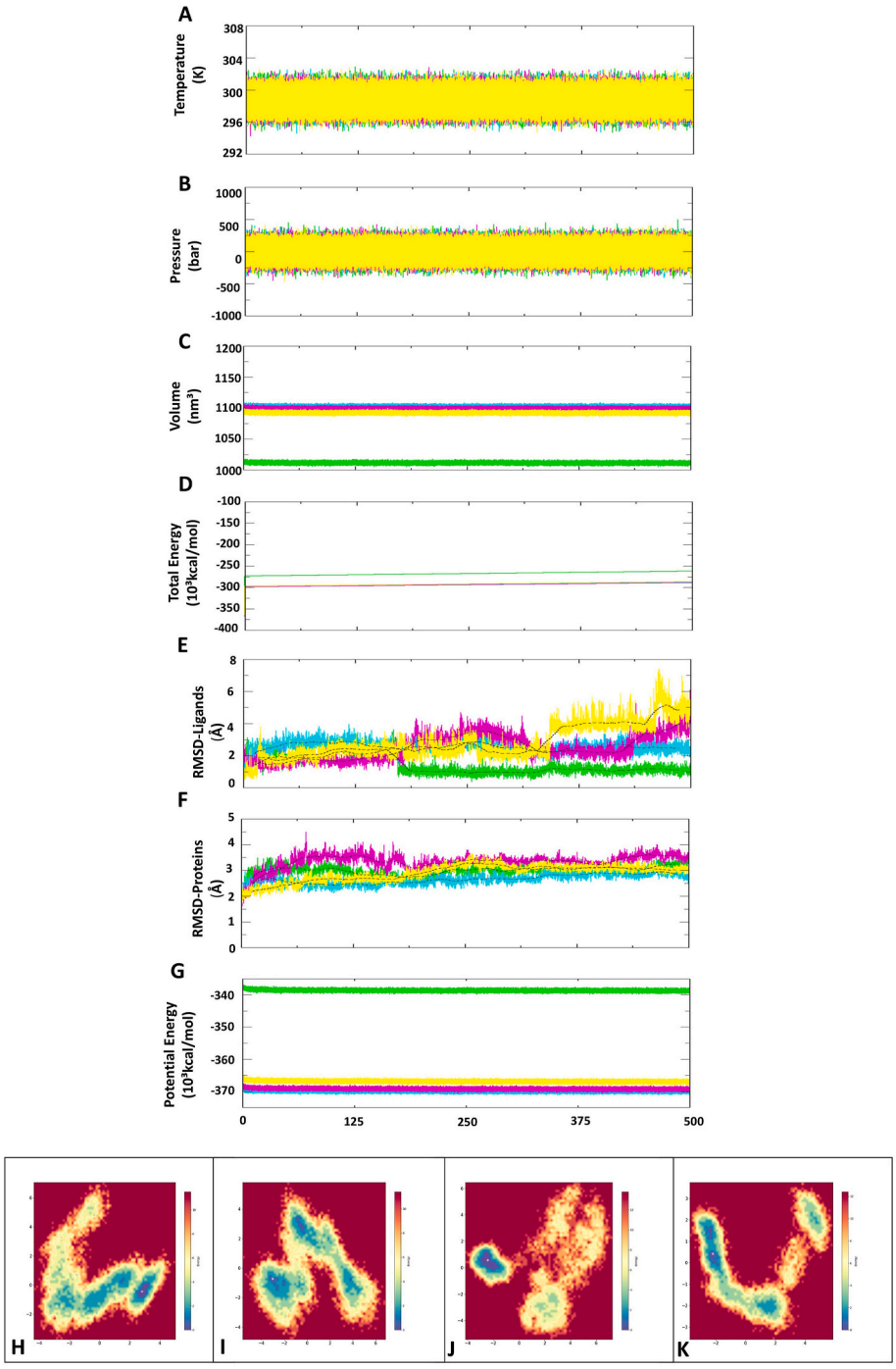

Fig. 5. Graphs showing parameters of Molecular Dynamics simulation of RdRp complexes with HHF318 molecule. (**A**) Temperature; (**B**) Pressure; (**C**) Volume; (**D**) Total energy; (**E**) Ligand RMSD; (**F**) Protein RMSD; (**G**) Potential energy. Plots for *SARS-CoV-2*, *SARS-CoV-1*, *MERS-CoV*, and *Bat-CoV* are shown in green, cyan, pink and yellow, respectively. Post MD free energy landscapes of RdRp-HHF318 complexes (**H**) *SARS-CoV-2* RdRp-HHF318, (**I**) *SARS-CoV-1* RdRp-HHF318, (**J**) *MERS-CoV* RdRp-HHF318, and (**K**) *Bat-CoV* RdRp-HHF318. Lowest energy and highest energy conformations are shown by dark blue and red, respectively. The white Asterix indicates the representative structure used for analysis.

primer RNA and NTP into the active site for catalysis (Fig. 2A). From a functional perspective, the catalytic reaction involves transfer of the alpha phosphate of the incoming nucleotide to the deprotonated 3′ OH group of the terminal nucleotide in the product strand incorporating it and pyrophosphate leaving the active site. This is enabled by the RdRp enzymes that have well defined channels for RNA entry, NTP entry and RNA exit [61–63]. Structural elements that are crucial for the incorporation of NTP to the elongating RNA are: (1) Asp 618, Tyr 619, Asp 760, Asp 761 that make coordination bonds with magnesium ions along with alpha phosphate oxygen of incoming nucleotide and 3′OH of the terminal nucleotide; (2) Recognition of incoming nucleotide by Lys 621, Cys 622, Asp 623 and Ser 682; (3) Basic residues Lys 545, Lys 551, Arg 553 and Arg 555 for positioning of negatively charged phosphates of NTP and RNA; (4) Arg 555 forms a pi-stacking with the nucleobase aligning it for catalysis as well as base pairing with the corresponding nucleotide in the template strand; (5) Basic residue Lys 545 forms a hydrogen bond with nucleobase, while Lys 551 interacts with the gamma phosphate of the NTP; (6) Residues Cys 813 and Ser 814 keeps

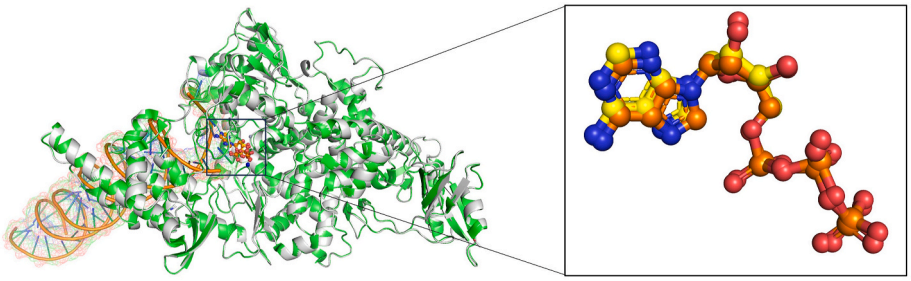

Fig. 6. Validation of docking methodology. Superimposition of Cryo-EM structure of RdRp from SARS-CoV-2 (green) with ATP (orange) (PDB Id:7UO7), with docked complex structure where the protein is shown in white and ligand is shown in yellow. RNA is shown as orange cartoon and Magnesium is shown as a blue sphere.

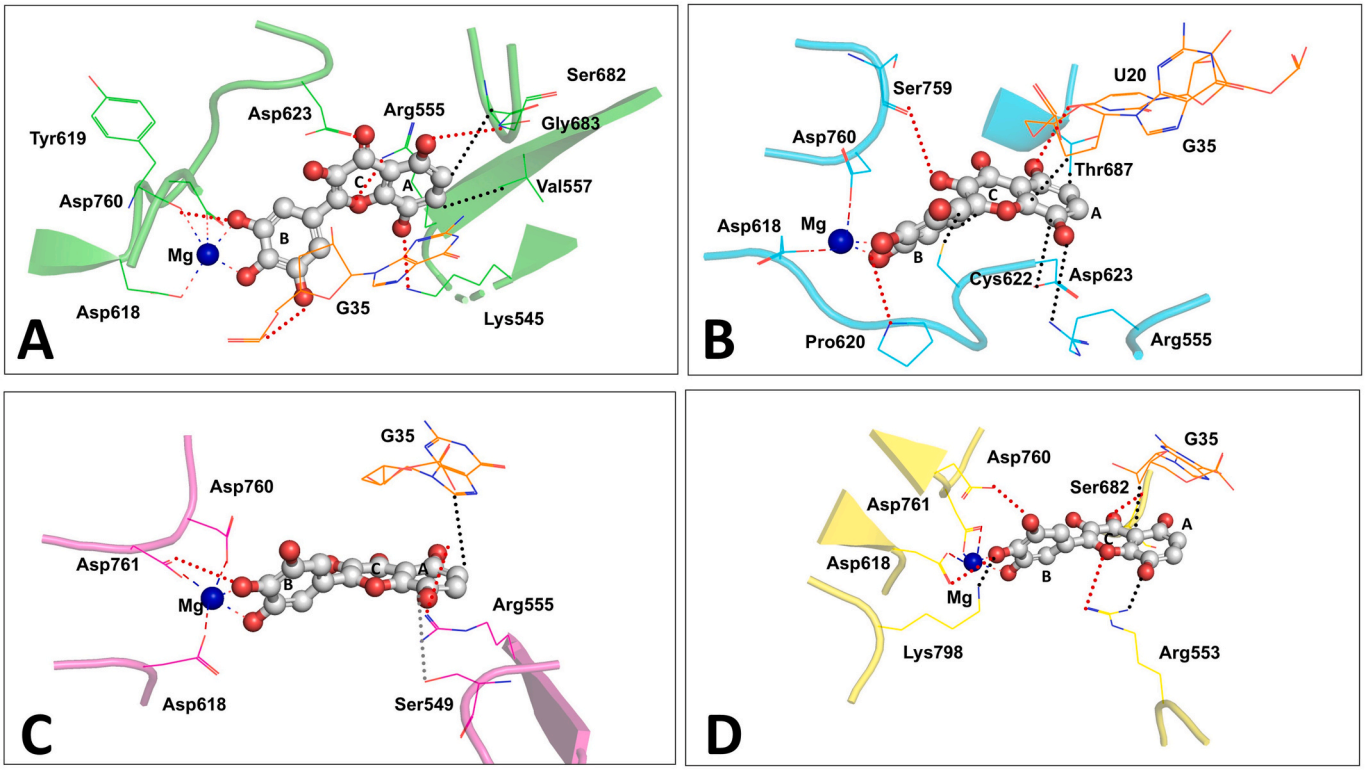

Fig. 7. HHF318 interactions with the RdRp enzymes (**A**) line and stick diagram showing interactions of HHF318 with *SARS-CoV-2* RdRp, (**B**) line and stick diagram showing interactions of HHF318 with *SARS-CoV-1* RdRp, (**C**) line and stick diagram showing interactions of HHF318 with *MERS-CoV* RdRp and (**D**) line and stick diagram showing interactions of HHF318 with *Bat-CoV* RdRp. Hydrogen bonds are shown as red dotted lines, Magnesium coordination bonds are shown as red-blue lines and hydrophobic interactions are shown as black dotted lines.

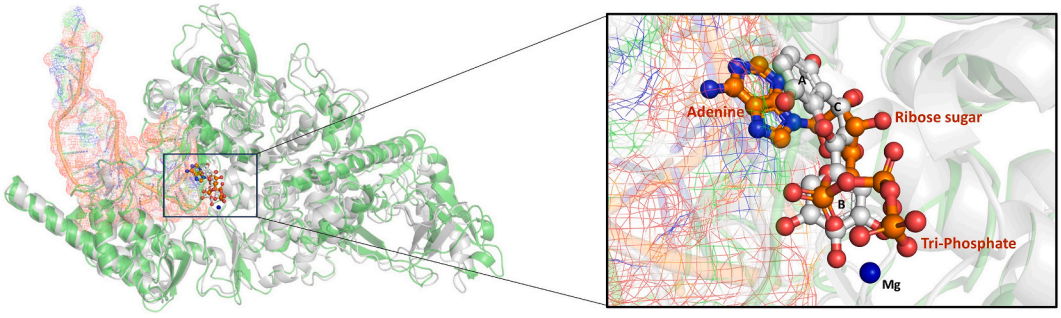

Fig. 8. Superimposed Cryo-EM structure of *SARS-CoV-2* RdRp with ATP (orange) and *SARS-CoV-2* RdRp with HHF318 (white) at the NTP binding site. RNA is shown as orange cartoon and magnesium is shown as blue sphere.

Table 1
Physico-chemical and pharmacokinetic properties of HHF318.

Formula	C15H10O8
Molecular weight	318.24
Aromatic heavy atoms	16
Hydrogen-bond acceptors	8
Hydrogen-bond donors	6
Total Polar Surface Area	151.59
Consensus Log P	1.02
Water solubility	Soluble
Gastro-intestinal absorption	Low
Blood Brain Barrier Permeation	No
Pgp substrate	No
CYP1A2 inhibitor	Yes
CYP2C19 inhibitor	No
CYP2C9 inhibitor	No
CYP2D6 inhibitor	Yes
CYP3A4 inhibitor	Yes
Lipinski #violations	1
Bioavailability Score	0.55
Lead likeness #violations	0
Synthetic Accessibility	3.29

the primer stand at the active site [21]. The above-mentioned structural features are presented in Fig. 2B.

3.4. Screening of inhibitors at NTP binding site of RdRp from SARS-CoV-2

Cryo-EM structure of *SARS-CoV-2* RdRp in a pre-catalytic conformation with ATP at the NTP binding site (PDB Id: 7UO7) was considered for modelling studies. Structure of RdRp of *SARS-CoV-2* enables the incorporation of NTP to the product RNA chain. NTP binding site, where the incoming nucleotide is recognized and positioned for catalysis, makes it an ideal site on the RdRp target for inhibitor screening. This NTP binding site of *SARS-CoV-2* RdRp was screened against natural molecule library. In the Virtual Screening Workflow, High-Throughput Virtual Screening identified 663 molecules. These were further refined using Standard Precision docking that yielded 66 top hits. Extra Precision docking was performed narrowing the selection to top 6 molecules. From among these Coconut ID: CNP0127177.0 which had the best docking score was chosen for further experiments. It occupies the NTP binding site in the vicinity of the elongating RNA and Magnesium ion (Fig. 4A). From a chemical perspective, this molecule is 3,3′,4′,5,5’,8-Hexahydroxyflavone, a flavonoid with molecular weight of 318.2Da, present in coffee. For the sake of convenience, this molecule will henceforth be referred to as HHF318 in the rest of the manuscript. Structurally, it comprises of two aromatic rings and one heterocyclic pyrone ring with six hydroxyl groups and one carbonyl group (Fig. 4B). As per the flavonoid nomenclature, the benzene rings are named Ring A and Ring B, and the heterocyclic ring is named Ring C [64]. Based on binding energies (ΔG), Dissociation constant (Kd) was estimated to be 1.8 nM. Interestingly, it is seen to be much more potent than the currently used nucleoside analogue inhibitors such as Remdesivir (5236 nM) and Favipiravir (159 nM). Also, the potency is better than the ATP, an NTP which has a Dissociation constant of 170 nM. Complexes of RdRp from *SARS-CoV-1, MERS-CoV*, and *Bat-CoV* with HHF318 were generated. These four RdRp complexes with HHF318 were subjected to 500ns of Molecular Dynamics simulation and stable conformation of the complexes were obtained. Trajectory analysis of MD simulation indicates that system quickly reached at target temperature of 300K and pressure of 1 bar and remained uniform throughout the equilibration stage (Fig. 5A–C). This indicated that the solvent and the ions had attained the right orientation around RdRp enzymes during period of equilibration. Under an NPT ensemble with constant number of atoms, pressure, and temperature, RdRp with the inhibitor molecule HHF318 closely replicates an experimental condition. Total energies were constant for all the four protein complexes indicating stability of the systems (Fig. 5, D). The RMSD plot was stable with average deviation of less than 2 Å from the mean indicating that the system of protein and solvent had reached a stable state with protein target in an optimum conformation (Fig. 5E and F). Protein RMSD plots for the complexes show that the backbone of the proteins from *SARS CoV-2* and *MERS-CoV* converged around 200ns, while that of *SARS-CoV-1* and *Bat-CoV* converged around 300ns. RMSD of HHF318 in the complexes of *SARS-CoV-2* and *SARS-CoV-1* remained stable throughout the simulations after convergence while that of *MERS-CoV* and *Bat-CoV* varied persistently indicating that HHF318 was not stably bound to the complexes. Values of potential energy indicates that the systems are stabilized and equipped for the molecular dynamics phase (Fig. 5, G). The free energy landscapes (FEL) of the first two principal components of the MD trajectory frames for the four complexes are shown in Fig. 5H–K, respectively. The FEL of *SARS-CoV-2* has a single well-defined deep blue basin indicating a stable conformational state with low energy compared to the other three enzyme complexes. Structures from the energy minima of each FEL, indicated by dark blue region were used for analysis of the interaction of HHF318 with each of the four RdRp enzymes. The Cryo EM structure of *SARS-CoV-2* with the ATP (**PDB Id:** 7UO7) was used for validating the modelling methodology. RMSD of docked complex of RdRp: ATP with the Cryo-EM structure is 0.4 Å (Fig. 6). This validates the docking methodology used in this study.

3.5. Interactions of HHF318 with RdRp

HHF318 binds to RdRp at the NTP binding site which has the 3’ strand of elongating RNA and co-factor magnesium ion. HHF318 forms an array of interactions with residues of RdRp from *SARS-CoV-2*. The details of the interactions are: Two hydroxyl groups from Ring B are involved in magnesium coordination along with residues Asp 618, Tyr

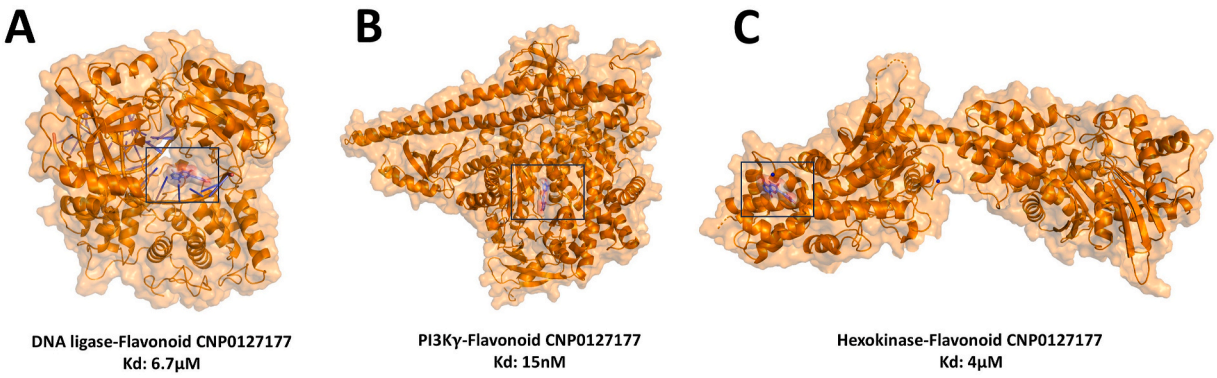

Fig. 9. Docked complexes of HHF318 with ATP binding human proteins. (**A**) DNA-Ligase-HHF318, (**B**) Pi3K–HHF318, (**C**) Hexokinase-HHF318. Dissociation constants (Kd) are indicated below each of the three complexes.

619, Asp 760. Hydroxyl group on Ring B forms a hydrogen bond with oxygen of phosphate group from the primer strand. Hydroxyl group in Ring A forms hydrogen bond with Lys 545. Carbonyl group on Ring C forms hydrogen bond with Asp 623, and hydroxyl group on Ring A makes hydrogen bond with the backbone of Gly 683. In addition, hydrophobic interactions exist between Carbon atoms of Ring A with main chain Carbon of Ser 682, and side chain of Val 557. Arg 555 makes cationic-π interaction with Ring A. Ring A additionally makes stacking interaction with nucleobase of G35 (Fig. 7A). The collated effect of these interactions is responsible for the strong binding affinity of HHF318 against RdRp of *SARS-CoV-2*. In the complex of *SARS-CoV-1* RdRp with HHF318, the major interactions include coordination of magnesium along with Asp 618 and Asp 760. Hydrogen bonds with Ser 759, Pro 620, and U-20 on the template strand. Hydrophobic interactions are made with Cys 622, Asp 623, Arg 555, Thr 687, and ribose sugar of G35 (Fig. 7B). Complex of *MERS-CoV* RdRp with HHF318 shows magnesium coordination along with Asp618, Asp760, and Asp761. Hydrogen bonded interactions exist between ligand and Asp 761 and Arg 555. In addition, hydrophobic interactions are with Ser549 and nucleobase of G35 (Fig. 7C). Lastly, Complex of *Bat-CoV* RdRp with HHF318 shows magnesium coordination along with Asp618 and Asp761. Hydrogen bonded interactions are seen with Asp760, Arg 553, Ser 682, and Asp 618. Hydrophobic interactions are with Lys798, Arg553, and G35 (Fig. 7D).

3.6. Comparison of superimposed structures of RdRp of SARS-CoV-2 with ATP and SARS-CoV-2 with HHF318

For a better understanding of the inhibition of *SARS-CoV-2* RdRp by HHF318, the structure complex was superimposed on the structure complex of *SARS-CoV-2* RdRp enzyme with ATP at the NTP binding site. It is seen that the main chain RMSD of the two complexes was 2 Å. Also, the two molecules in the two complexes too were superimposed on one another, adjacent to the magnesium ion for coordination (Fig. 8). The other interesting findings are: (1) Benzene (Ring A) with two hydroxyl group of HHF318 is within 3 Å distance from the adenine base of ATP; (2) Both molecules, HHF318 and ATP are positioned adjacent to the guanine base of the RNA in the primer strand; (3) heterocyclic pyrone (Ring C) of the HHF318 is superimposed on the ribose sugar of ATP, and (4) Benzene (Ring B) with three hydroxyl group comes to lie adjacent to the hydrophilic phosphate group (Fig. 8). This clearly establishes that the physio-chemical features of HHF318 makes it a potential competitive inhibitor of nucleotide binding at NTP binding site of RdRp.

3.7. Physico-chemical and pharmacokinetic properties of HHF318

Physico-chemical and pharmacokinetic properties of a ligand is the main stay for its development into a drug molecule. Molecule HHF318 was evaluated for the same and the estimated Physico-chemical and pharmacokinetic properties is presented in Table 1. Some of the notable aspects are: (1) its highly polar nature makes it water soluble; (2) compound is moderately lipid soluble explaining the low GI absorption and blood brain barrier non-permeability; (3) High aromatic heavy atom count could possibly help in forming strong interactions with biological target, but and also increase inhibition of CYP1A2, CYP2D6, and CYP3A4 enzymes in the liver that could cause drug-drug interactions; (4) compound being a non-P-glycoprotein substrate could improve its bioavailability; and (5) The Lipinski rule compliance, moderate bioavailability score, no violations in lead-likeness and relative easiness in synthesizing makes HHF318 an ideal candidate for further optimisation in drug discovery against COVID19.

3.8. Interactions of HHF318 with secondary drug targets in the human body

In order to analyse the specificity of HHF318 binding to RdRp enzyme, the molecule was docked with certain ATP binding human proteins like DNA Ligase, PI3K and Hexokinase. The molecule binds at the ATP binding site of the proteins (Fig. 9). The theoretical Kd of binding of HHF318molecule with these enzymes are 6.7 μM, 15 nM and 4 μM, respectively. These values are higher than 1.8 nM which we have estimated for the same molecule against RdRp from *SARS-CoV-2*. This is indicative of the fact that the molecule is not only potent but also very specific against the drug target of RdRp from *SARS-CoV-2*.

3.9. Limitation of the study

This is a computation based structural bioinformatic study. Crystallization experiments, enzyme inhibition assays and *ex-vivo* studies would help to validate the credentials of the identified molecule for it to be translated into therapeutics for COVID 19 disease.

4. Conclusion

RNA Dependent RNA polymerase enzymes across the Coronaviridae family have similar sequence and three-dimensional fold. However, variations in analogous residue positions play a role in the compactness thereby imparting greater stability of RdRp enzyme from *SARS-CoV-2* compared to its homologs. Structure Based Drug Screening helped to identify the flavonoid molecule with Coconut ID: CNP0127177.0 (HHF318) that has binding affinity in low nano-molar range against RdRp from *SARS-CoV-2*. The strong affinity stems from the cumulative effect of an array of interactions including cationic-π, and π-stacking with protein and RNA, respectively. This molecule engages with residues that are crucial for functions such as magnesium coordination, nucleotide recognition and positioning, and catalysis. Additionally, it has a lower potency for human ATP binding proteins, making it an ideal drug candidate for COVID19.

CRediT authorship contribution statement

Shamiya Anwar Kizhakkiniyakath: Methodology. **Tejaswini Choudhury:** Methodology. **Madhan Vishal Rajan:** Methodology. **Sagar Rathee:** Methodology. **Basant Meena:** Methodology. **Gururao Hariprasad:** Writing – review & editing, Writing – original draft, Visualization, Validation, Supervision, Software, Resources, Project administration, Methodology, Investigation, Funding acquisition, Formal analysis, Data curation, Conceptualization.

Data availability statement

The models are available in ModelArchive (modelarchive.org) with the accession codes: RdRp from *SARS-CoV-2* with molecule HHF318 (ma-6pwl6); RdRp from *SARS-CoV-1* with molecule HHF318 (ma-tknqc), RdRp from *MERS-CoV* with molecule HHF318 (ma-z5jqd), RdRp from *Bat-CoV* with molecule HHF318 (ma-gcwge).

Declaration of competing interest

Authors report no conflict of interest in this work.

Appendix A. Supplementary data

Supplementary data to this article can be found online at https://doi.org/10.1016/j.bbrep.2025.101975.

References

[1] L. Duan, G. Zhu, Psychological interventions for people affected by the COVID-19 epidemic, Lancet Psychiatry 7 (2020) 300–302, https://doi.org/10.1016/S2215-0366(20)30073-0.
[2] S.M.R. Hashemian, A. Sheida, M. Taghizadieh, M.Y. Memar, M.R. Hamblin, H. Bannazadeh Baghi, J. Sadri Nahand, Z. Asemi, H. Mirzaei, Paxlovid

(Nirmatrelvir/Ritonavir): a new approach to Covid-19 therapy? Biomed. Pharmacother. 162 (2023) 114367 https://doi.org/10.1016/j.biopha.2023.114367.
[3] M. Day, Covid-19: ibuprofen should not be used for managing symptoms, say doctors and scientists, Br. Med. J. 368 (2020) m1086, https://doi.org/10.1136/bmj.m1086.
[4] C. For D.E. and Research, FDA Cautions against Use of Hydroxychloroquine or Chloroquine for COVID-19 outside of the Hospital Setting or a Clinical Trial Due to Risk of Heart Rhythm Problems, FDA (2023). https://www.fda.gov/drugs/drug-safety-and-availability/fda-cautions-against-use-hydroxychloroquine-or-chloroquine-covid-19-outside-hospital-setting-or (accessed March 8, 2024).
[5] S. Atluri, L. Manchikanti, J.A. Hirsch, Expanded umbilical cord mesenchymal stem cells (UC-MSCs) as a therapeutic strategy in managing critically ill COVID-19 patients: the case for compassionate use, Pain Physician 23 (2020) E71–E83.
[6] S. Ekins, T.R. Lane, P.B. Madrid, Tilorone: a broad-spectrum antiviral invented in the USA and commercialized in Russia and beyond, Pharm. Res. 37 (2020) 71, https://doi.org/10.1007/s11095-020-02799-8.
[7] D. Gurwitz, Angiotensin receptor blockers as tentative SARS-CoV-2 therapeutics, Drug Dev. Res. 81 (2020) 537–540, https://doi.org/10.1002/ddr.21656.
[8] S. Jawhara, Could intravenous immunoglobulin collected from recovered coronavirus patients protect against COVID-19 and strengthen the immune system of new patients? Int. J. Mol. Sci. 21 (2020) 2272, https://doi.org/10.3390/ijms21072272.
[9] H. Kang, C.K. Kang, J.H. Im, Y. Cho, D.Y. Kang, J.-Y. Lee, Adverse drug events associated with remdesivir in real-world hospitalized patients with COVID-19, including vulnerable populations: a retrospective multicenter study, J. Kor. Med. Sci. 38 (2023) e346, https://doi.org/10.3346/jkms.2023.38.e346.
[10] M.A. Ahmed-Khan, G. Matar, K. Coombes, K. Moin, B.M. Joseph, C.M. Funk, M. A. Ahmed-Khan, G. Matar, K. Coombes, K. Moin, B.M.N. Joseph, C.M. Funk, Remdesivir-associated acute liver failure in a COVID-19 patient: a case report and literature review, Cureus 15 (2023), https://doi.org/10.7759/cureus.34221.
[11] Information on COVID-19 Treatment, Prevention and Research, COVID-19 Treatment Guidelines. https://www.covid19treatmentguidelines.nih.gov/ (accessed March 8, 2024).
[12] S. Batool, K. Vuthaluru, A. Hassan, O. Bseiso, Z. Tehseen, G. Pizzorno, Y. Rodriguez Reyes, F. Saleem, Efficacy and Safety of Favipiravir in Treating COVID-19 Patients: A Meta-Analysis of Randomized Control Trials, Cureus 15 e33676. https://doi.org/10.7759/cureus.33676.
[13] A. Nourian, H. Khalili, Z. Ahmadinejad, H. Emadi Kouchak, S. Jafari, S.A. Dehghan Manshadi, M. Rasolinejad, A. Kebriaeezadeh, Efficacy and safety of sofosbuvir/ledipasvir in treatment of patients with COVID-19; A randomized clinical trial, Acta Biomed. 91 (2020) e2020102, https://doi.org/10.23750/abm.v91i4.10877.
[14] J.G. Julander, J.F. Demarest, R. Taylor, B.B. Gowen, D.M. Walling, A. Mathis, Y. S. Babu, An update on the progress of galidesivir (BCX4430), a broad-spectrum antiviral, Antivir. Res. 195 (2021) 105180, https://doi.org/10.1016/j.antiviral.2021.105180.
[15] J. Zhao, S. Guo, D. Yi, Q. Li, L. Ma, Y. Zhang, J. Wang, X. Li, F. Guo, R. Lin, C. Liang, Z. Liu, S. Cen, A cell-based assay to discover inhibitors of SARS-CoV-2 RNA dependent RNA polymerase, Antivir. Res. 190 (2021) 105078, https://doi.org/10.1016/j.antiviral.2021.105078.
[16] X. Xu, Y. Chen, X. Lu, W. Zhang, W. Fang, L. Yuan, X. Wang, An update on inhibitors targeting RNA-dependent RNA polymerase for COVID-19 treatment: promises and challenges, Biochem. Pharmacol. 205 (2022) 115279, https://doi.org/10.1016/j.bcp.2022.115279.
[17] E.P. Tchesnokov, C.J. Gordon, E. Woolner, D. Kocinkova, J.K. Perry, J.Y. Feng, D. P. Porter, M. Götte, Template-dependent inhibition of coronavirus RNA-dependent RNA polymerase by remdesivir reveals a second mechanism of action, J. Biol. Chem. 295 (2020) 16156–16165, https://doi.org/10.1074/jbc.AC120.015720.
[18] P. Ahlquist, A.O. Noueiry, W.-M. Lee, D.B. Kushner, B.T. Dye, Host factors in positive-strand RNA virus genome replication, J. Virol. 77 (2003) 8181–8186, https://doi.org/10.1128/jvi.77.15.8181-8186.2003.
[19] A. Salonen, T. Ahola, L. Kääriäinen, Viral RNA replication in association with cellular membranes, Curr. Top. Microbiol. Immunol. 285 (2005) 139–173, https://doi.org/10.1007/3-540-26764-6_5.
[20] W.A. Miller, G. Koev, Synthesis of subgenomic RNAs by positive-strand RNA viruses, Virology 273 (2000) 1–8, https://doi.org/10.1006/viro.2000.0421.
[21] B.F. Malone, J.K. Perry, P.D.B. Olinares, H.W. Lee, J. Chen, T.C. Appleby, J.Y. Feng, J.P. Bilello, H. Ng, J. Sotiris, M. Ebrahim, E.Y.D. Chua, J.H. Mendez, E.T. Eng, R. Landick, M. Götte, B.T. Chait, E.A. Campbell, S.A. Darst, Structural basis for substrate selection by the SARS-CoV-2 replicase, Nature 614 (2023) 781–787, https://doi.org/10.1038/s41586-022-05664-3.
[22] W. Yin, C. Mao, X. Luan, D.-D. Shen, Q. Shen, H. Su, X. Wang, F. Zhou, W. Zhao, M. Gao, S. Chang, Y.-C. Xie, G. Tian, H.-W. Jiang, S.-C. Tao, J. Shen, Y. Jiang, H. Jiang, Y. Xu, S. Zhang, Y. Zhang, H.E. Xu, Structural basis for inhibition of the RNA-dependent RNA polymerase from SARS-CoV-2 by remdesivir, Science 368 (2020) 1499–1504, https://doi.org/10.1126/science.abc1560.
[23] Y. Gao, L. Yan, Y. Huang, F. Liu, Y. Zhao, L. Cao, T. Wang, Q. Sun, Z. Ming, L. Zhang, J. Ge, L. Zheng, Y. Zhang, H. Wang, Y. Zhu, C. Zhu, T. Hu, T. Hua, B. Zhang, X. Yang, J. Li, H. Yang, Z. Liu, W. Xu, L.W. Guddat, Q. Wang, Z. Lou, Z. Rao, Structure of the RNA-dependent RNA polymerase from COVID-19 virus, Science 368 (2020) 779–782, https://doi.org/10.1126/science.abb7498.
[24] K. Glab-ampai, K. Kaewchim, T. Thavorasak, T. Saenlom, W. Thepsawat, K. Mahasongkram, K. Thueng-In, N. Sookrung, W. Chaicumpa, M. Chulanetra, Targeting emerging RNA viruses by engineered human superantibody to hepatitis C virus RNA-dependent RNA polymerase, Front. Microbiol. 13 (2022), https://doi.org/10.3389/fmicb.2022.926929.
[25] M.C. Dias, D.C.G.A. Pinto, A.M.S. Silva, Plant flavonoids: chemical characteristics and biological activity, Molecules 26 (2021) 5377, https://doi.org/10.3390/molecules26175377.
[26] S. Safe, A. Jayaraman, R.S. Chapkin, M. Howard, K. Mohankumar, R. Shrestha, Flavonoids: structure–function and mechanisms of action and opportunities for drug development, Toxicol. Res. 37 (2021) 147–162, https://doi.org/10.1007/s43188-020-00080-z.
[27] K.E. Heim, A.R. Tagliaferro, D.J. Bobilya, Flavonoid antioxidants: chemistry, metabolism and structure-activity relationships, J. Nutr. Biochem. 13 (2002) 572–584, https://doi.org/10.1016/S0955-2863(02)00208-5.
[28] A.N. Panche, A.D. Diwan, S.R. Chandra, Flavonoids: an overview, J. Nutr. Sci. 5 (2016) e47, https://doi.org/10.1017/jns.2016.41.
[29] S. Kumar, A.K. Pandey, Chemistry and biological activities of flavonoids: an overview, Sci. World J. 2013 (2013) 162750, https://doi.org/10.1155/2013/162750.
[30] G. Hariprasad, M. Kumar, P. Kaur, T.P. Singh, R.P. Kumar, Human group III PLA2 as a drug target: structural analysis and inhibitor binding studies, Int. J. Biol. Macromol. 47 (2010) 496–501, https://doi.org/10.1016/j.ijbiomac.2010.07.004.
[31] A. Goswami, T. Koley, M.V. Rajan, P. Madhuri, N. Upadhyay, U. Das, M. Kumar, A. S. Ethayathulla, G. Hariprasad, Structural modelling of platelet activating factor acetyl hydrolase in leishmania donovani, trypanosoma cruzi, and trypanosoma brucei: implications on therapeutics for leishmaniasis, chagas disease, and sleeping sickness, Infect. Drug Resist. 16 (2023) 2117–2128, https://doi.org/10.2147/IDR.S403411.
[32] E.W. Sayers, E.E. Bolton, J.R. Brister, K. Canese, J. Chan, D.C. Comeau, R. Connor, K. Funk, C. Kelly, S. Kim, T. Madej, A. Marchler-Bauer, C. Lanczycki, S. Lathrop, Z. Lu, F. Thibaud-Nissen, T. Murphy, L. Phan, Y. Skripchenko, T. Tse, J. Wang, R. Williams, B.W. Trawick, K.D. Pruitt, S.T. Sherry, Database resources of the national center for biotechnology information, Nucleic Acids Res. 50 (2022) D20–D26, https://doi.org/10.1093/nar/gkab1112.
[33] S.F. Altschul, W. Gish, W. Miller, E.W. Myers, D.J. Lipman, Basic local alignment search tool, J. Mol. Biol. 215 (1990) 403–410, https://doi.org/10.1016/S0022-2836(05)80360-2.
[34] F. Sievers, A. Wilm, D. Dineen, T.J. Gibson, K. Karplus, W. Li, R. Lopez, H. McWilliam, M. Remmert, J. Söding, J.D. Thompson, D.G. Higgins, Fast, scalable generation of high-quality protein multiple sequence alignments using Clustal Omega, Mol. Syst. Biol. 7 (2011) 539, https://doi.org/10.1038/msb.2011.75.
[35] H.M. Berman, J. Westbrook, Z. Feng, G. Gilliland, T.N. Bhat, H. Weissig, I. N. Shindyalov, P.E. Bourne, The protein Data Bank, Nucleic Acids Res. 28 (2000) 235–242, https://doi.org/10.1093/nar/28.1.235.
[36] R.A. Laskowski, M.W. MacArthur, D.S. Moss, J.M. Thornton, PROCHECK: a program to check the stereochemical quality of protein structures, J. Appl. Crystallogr. 26 (1993) 283–291, https://doi.org/10.1107/S0021889892009944.
[37] J. Bowie, R. Luethy, D. Eisenberg, A method to identify protein sequences that fold into a known three-dimensional structure, Science (New York, N.Y.) 253 (1991) 164–170, https://doi.org/10.1126/science.1853201.
[38] R. Lüthy, J.U. Bowie, D. Eisenberg, Assessment of protein models with three-dimensional profiles, Nature 356 (1992) 83–85, https://doi.org/10.1038/356083a0.
[39] C. Colovos, T. Yeates, C. Colovos, T.O. Yeates, Verification of protein structures: patterns of nonbonded atomic interactions, Protein Sci. 2, Protein Sci. : Pub. Protein Soc. 2 (1993) 1511–1519, https://doi.org/10.1002/pro.5560020916, 1511–9.
[40] D. Systèmes, Free Download: BIOVIA Discovery Studio Visualizer, Dassault Systèmes, 2020. https://discover.3ds.com/discovery-studio-visualizer-download. (Accessed 11 October 2024).
[41] A. Waterhouse, M. Bertoni, S. Bienert, G. Studer, G. Tauriello, R. Gumienny, F. T. Heer, T.A.P. de Beer, C. Rempfer, L. Bordoli, R. Lepore, T. Schwede, SWISS-MODEL: homology modelling of protein structures and complexes, Nucleic Acids Res. 46 (2018) W296–W303, https://doi.org/10.1093/nar/gky427.
[42] C. Combet, M. Jambon, G. Deléage, C. Geourjon, Geno3D: automatic comparative molecular modelling of protein, Bioinformatics 18 (2002) 213–214, https://doi.org/10.1093/bioinformatics/18.1.213.
[43] L.A. Kelley, S. Mezulis, C.M. Yates, M.N. Wass, M.J.E. Sternberg, The Phyre2 web portal for protein modeling, prediction and analysis, Nat. Protoc. 10 (2015) 845–858, https://doi.org/10.1038/nprot.2015.053.
[44] G. Madhavi Sastry, M. Adzhigirey, T. Day, R. Annabhimoju, W. Sherman, Protein and ligand preparation: parameters, protocols, and influence on virtual screening enrichments, J. Comput. Aided Mol. Des. 27 (2013) 221–234, https://doi.org/10.1007/s10822-013-9644-8.
[45] K. Zandi, K. Musall, A. Oo, D. Cao, B. Liang, P. Hassandarvish, S. Lan, R.L. Slack, K. A. Kirby, L. Bassit, F. Amblard, B. Kim, S. AbuBakar, S.G. Sarafianos, R.F. Schinazi, Baicalein and baicalin inhibit SARS-CoV-2 RNA-dependent-RNA polymerase, Microorganisms 9 (2021) 893, https://doi.org/10.3390/microorganisms9050893.
[46] O.A. Chaves, N. Fintelman-Rodrigues, X. Wang, C.Q. Sacramento, J.R. Temerozo, A.C. Ferreira, M. Mattos, F. Pereira-Dutra, P.T. Bozza, H.C. Castro-Faria-Neto, J. J. Russo, J. Ju, T.M.L. Souza, Commercially available flavonols are better SARS-CoV-2 inhibitors than isoflavone and flavones, Viruses 14 (2022) 1458, https://doi.org/10.3390/v14071458.
[47] Y. Wu, D. Crich, S.D. Pegan, L. Lou, M.C. Hansen, C. Booth, E. Desrochers, L. N. Mullininx, E.B. Starling, K.Y. Chang, Z.-R. Xie, Polyphenols as potential inhibitors of SARS-CoV-2 RNA dependent RNA polymerase (RdRp), Molecules 26 (2021), https://doi.org/10.3390/molecules26247438.
[48] M. Sorokina, P. Merseburger, K. Rajan, M.A. Yirik, C. Steinbeck, COCONUT online: collection of open natural products database, J. Cheminf. 13 (2021) 2, https://doi.org/10.1186/s13321-020-00478-9.

[49] LigPrep, Schrödinger. https://www.schrodinger.com/platform/products/ligprep/(accessed October 11, 2024).
[50] M. Sastry, J.F. Lowrie, S.L. Dixon, W. Sherman, Large-Scale systematic analysis of 2D fingerprint methods and parameters to improve virtual screening enrichments, J. Chem. Inf. Model. 50 (2010) 771–784, https://doi.org/10.1021/ci100062n.
[51] T.A. Halgren, R.B. Murphy, R.A. Friesner, H.S. Beard, L.L. Frye, W.T. Pollard, J. L. Banks, Glide: a new approach for rapid, accurate docking and scoring. 2. Enrichment factors in database screening, J. Med. Chem. 47 (2004) 1750–1759, https://doi.org/10.1021/jm030644s.
[52] PyMOL | pymol.org,. https://www.pymol.org/(accessed October 11, 2024).
[53] K. Bowers, E. Chow, H. Xu, R. Dror, M. Eastwood, B. Gregersen, J. Klepeis, I. Kolossvary, M. Moraes, F. Sacerdoti, J. Salmon, Y. Shan, D. Shaw, Scalable Algorithms for Molecular Dynamics Simulations on Commodity Clusters, in: ACM/IEEE SC 2006 Conference (SC'06), https://doi.org/10.1109/SC.2006.54.
[54] E. Harder, W. Damm, J. Maple, C. Wu, M. Reboul, J.Y. Xiang, L. Wang, D. Lupyan, M.K. Dahlgren, J.L. Knight, J.W. Kaus, D.S. Cerutti, G. Krilov, W.L. Jorgensen, R. Abel, R.A. Friesner, OPLS3: a force field providing broad coverage of drug-like small molecules and proteins, J. Chem. Theor. Comput. 12 (2016) 281–296, https://doi.org/10.1021/acs.jctc.5b00864.
[55] W.G. Hoover, Canonical dynamics: equilibrium phase-space distributions, Phys. Rev. A 31 (1985) 1695–1697, https://doi.org/10.1103/PhysRevA.31.1695.
[56] G.J. Martyna, D.J. Tobias, M.L. Klein, Constant pressure molecular dynamics algorithms, J. Chem. Phys. 101 (1994) 4177–4189, https://doi.org/10.1063/1.467468.
[57] B. Hess, H. Bekker, H.J.C. Berendsen, J.G.E.M. Fraaije, LINCS: a linear constraint solver for molecular simulations, J. Comput. Chem. 18 (1997) 1463–1472.
[58] M. Tuckerman, B.J. Berne, G.J. Martyna, Reversible multiple time scale molecular dynamics, J. Chem. Phys. 97 (1992) 1990–2001, https://doi.org/10.1063/1.463137.
[59] R.T. McGibbon, K.A. Beauchamp, M.P. Harrigan, C. Klein, J.M. Swails, C. X. Hernández, C.R. Schwantes, L.-P. Wang, T.J. Lane, V.S. Pande, MDTraj: a modern open library for the analysis of molecular dynamics trajectories, Biophys. J. 109 (2015) 1528–1532, https://doi.org/10.1016/j.bpj.2015.08.015.
[60] J. Palma, G. Pierdominici-Sottile, On the uses of PCA to characterise molecular dynamics simulations of biological macromolecules: basics and tips for an effective use, ChemPhysChem 24 (2023) e202200491, https://doi.org/10.1002/cphc.202200491.
[61] J. Aranda, M. Wieczór, M. Terrazas, I. Brun-Heath, M. Orozco, Mechanism of reaction of RNA-dependent RNA polymerase from SARS-CoV-2, Chem Catal. 2 (2022) 1084–1099, https://doi.org/10.1016/j.checat.2022.03.019.
[62] Y. Jiang, W. Yin, H.E. Xu, RNA-dependent RNA polymerase: structure, mechanism, and drug discovery for COVID-19, Biochem. Biophys. Res. Commun. 538 (2021) 47–53, https://doi.org/10.1016/j.bbrc.2020.08.116.
[63] D. Garriga, C. Ferrer-Orta, J. Querol-Audí, B. Oliva, N. Verdaguer, Role of motif B loop in allosteric regulation of RNA-dependent RNA polymerization activity, J. Mol. Biol. 425 (2013) 2279–2287, https://doi.org/10.1016/j.jmb.2013.03.034.
[64] G.R. Beecher, Overview of dietary flavonoids: nomenclature, occurrence and intake, J. Nutr. 133 (2003) 3248S–3254S, https://doi.org/10.1093/jn/133.10.3248S.